

Algorithm for Solving Non-Stationary Heat Conduction Problem for Design of a Technical Device

A. Ayriyan^{a,*}, J. Buša Jr.^b, E.E. Donets^c, H. Grigorian^{a,d}, J. Pribiš^{a,b}

^aLaboratory of Information Technologies, JINR, Dubna, Russia

^bDepartment of Mathematics and Theoretical Informatics, TU of Košice, Košice, Slovakia

^cVeksler and Baldin Laboratory of High Energy Physics, JINR, Dubna, Russia

^dDepartment of Theoretical Physics, Yerevan State University, Yerevan, Armenia

Abstract

A model of a multilayer device with non-trivial geometrical and material structure and its working process is suggested. The thermal behavior of the device as one principle characteristic is simulated. The algorithm for solving the non-stationary heat conduction problem with a time-dependent periodical heating source is suggested. The algorithm is based on finite difference explicit–implicit method. The OpenCL realization of the algorithm is discussed. The results show that the chosen characteristics of the device configuration are suitable for the working requirements for application.

Keywords: Heat equation, Partial differential equation, Finite-difference scheme, Mathematical modeling, OpenCL realization

1. Introduction

In modern science and technology of thermal conductivity, there is a very common phenomena for the study of complex objects with complex geometric and physical structure. The main goal of this work is to suggest a model of temperature evolution for a multilayer cylindrical object, which has application in electron-string sources of multiply charged ions [1, 2]. The function of this device is pulse feeding (in the millisecond range) the working gases into the working space of the ion source.

The key character of the device working process is the temperature regime. When on the surface, the temperature changes periodically during the time around the critical temperature of working gases (T_{crit}). The principle of the operation is to select the necessary substance (working gases) from the input mixture of gases and to transfer it to the ion source. The mechanism is based on the difference of the evaporation temperatures of species of the mixture. The working gases have the lowest temperature of evaporation. The thermal process is governed by the periodic passage of electric current through one of the layer of the object. The period of the process is

*Corresponding author

Email address: ayriyan@jinr.ru (A. Ayriyan)

requested to be $t_{prd} = t_{src} + t_{clg}$. The period is divided in two parts: when the device evaporates working gases from its surface ($T > T_{crit}$) and when it condensates working gases on the surface ($T < T_{crit}$). The device itself works in the cryogenic temperature range from temperature of liquid helium ($T = 4.2$ K) up to temperature of liquid nitrogen ($T = 78$ K). The device structure has a cylindrical symmetry; therefore, the heat conductivity inside it can be simulated by a model with two spatial cylindrical coordinates, r and z , and time variables (Fig. 1). Similar but more simple model has been discussed in [3] and [4].

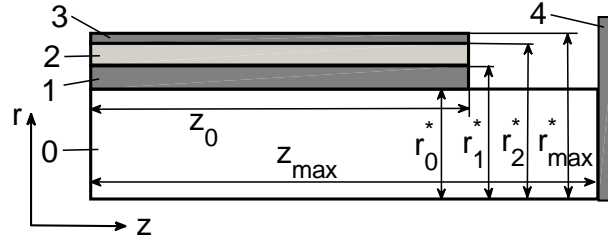


Figure 1: Schematic view of the object slice. The slice of the object: 0 – cooler, 1 – electrical insulator, 2 – heat source (conductive layer), 3 – external insulator, 4 – liquid helium temperature terminal with $T = 4.2$ K.

2. Main Equations and Boundary Conditions

The thermal processes in the object can be described by the following system of parabolic partial differential equations with temperature depended coefficients [5]:

$$\rho_m c v_m(T) \frac{\partial T}{\partial t} = \frac{1}{r} \frac{\partial}{\partial r} \left(r \lambda_m(T) \frac{\partial T}{\partial r} \right) + \frac{\partial}{\partial z} \left(\lambda_m(T) \frac{\partial T}{\partial z} \right) + X_m(T, t), \quad (1)$$

where $r \in [0, r_{max}(z)]$, $z \in [0, z_{max}(r)]$ (or $(r, z) \in \Omega$) and $t \geq 0$. The object consists of different materials in construction with different densities and thermal coefficients; thus, the index m is introduced for each material ($m = 0$ – cooler (copper), $m = 1$ – electrical insulator, $m = 2$ – heat source (graphite), $m = 3$ – external insulator). In the frame of this work, physical and engineering needs of the object geometry are not discussed. The source function in Eq. (1) is $X_m(T) \equiv 0$ for the layers $m = 0, 1$, and 3 (there is no source) and has a periodical time dependence:

$$X_2(T, t) = 10^7 V^{-1} I^2(t) \chi(T), \quad (2)$$

where V is volume of the object in units cm^3 , and

$$\chi(T) = 1.8 \left(\frac{T}{\text{K}} \right)^{-1/2} \text{Om}, \quad (3)$$

$$I(t) = I_0 v(t) p(t), \quad (4)$$

$$v(t) = \begin{cases} 1, & nt_{prd} \leq t < nt_{prd} + t_{src} \\ 0, & nt_{prd} + t_{src} \leq t < (n+1)t_{prd} \end{cases}, \quad (5)$$

here $n \in \mathbb{N}_0$.

Function $\nu(t)$ has a uniform rectangular waveform [6], and $p(t)$ is a model of the transient response function [7] for the turn-on process. In a simple case, it can be the Heaviside step function. For this work function $p(t)$ is discussed in chapter 3.1. In the formulas, $I(t)$ stands for electric current in the graphite slice along z direction, $I_0 = 10^3$ mA. In a common case, the thermal coefficients are nonlinear functions of the temperature and the spatial coordinates with discontinuities of first kind ($m + 1$ points of discontinuities).

The initial condition is given by

$$T(r, z, t = 0) = T_0, \quad (6)$$

where $T_0 \equiv 4.2$ K (liquid helium temperature) and the boundary conditions are taken as

$$\begin{cases} \frac{\partial T}{\partial \mathbf{n}} = 0 & \forall (r, z) \in \delta\Omega \setminus \{(r, z) : z = z_{max}\}, \\ T = T_0 & \forall (r, z) \in \{(r, z) : z = z_{max}\}, \end{cases} \quad (7)$$

where $\delta\Omega$ is the bound of the Ω , and \mathbf{n} – the normal vector of $\delta\Omega$. The temperature at the right side is always equal to T_0 because of contact with liquid helium.

The parameter ρ and the functions c_V , λ and $X_i = X(T_i)$ have discontinuities of first kind at the following surfaces with radii: r_0^* , r_1^* and r_2^* in the interval $[0..r_{max}]$. Conjugation conditions between materials are considered to be ideal:

$$\begin{cases} T|_{r=r_m^*-0} = T|_{r=r_m^*+0}, \\ -\lambda_m(T) \frac{\partial T}{\partial r} \Big|_{r=r_m^*-0} = -\lambda_{m+1}(T) \frac{\partial T}{\partial r} \Big|_{r=r_m^*+0}, \end{cases} \quad (8)$$

where r_m^* are points of the border between the materials m and $m + 1$ (discontinuity points), here $m = 0, 1, 2$.

3. Numerical Algorithm

The initial-boundary-value problem Eq. (1)–(7) has been approximated by the following mixed explicit–implicit finite difference scheme [8, 11]:

$$\rho_{i,j} c_{V,i,j} \frac{\widehat{T}_{i,j} - T_{i,j}}{\tau} = \Lambda_i [\widehat{T}_{i,j}] + \Lambda_j [T_{i,j}] + X_{i,j}. \quad (9)$$

where $\widehat{T}_{i,j}$ – temperature on the next time step, $T_{i,j}$ – temperature on the current time step, τ – time-step.

Numerical solutions of Eq. (9) can be performed using the special non-uniform grid [8]:

$$\begin{aligned} \bar{\omega} &= \{(t, x, z) | \quad 0 \leq t < \infty, \quad t_i = k \cdot h_t, \quad k \in \mathbb{N}_0; \\ &\quad 0 \leq r \leq r_{max}, \quad r_{i+1} = r_i + h_{i+1}, \quad i = 0 \dots N_j - 1; \\ &\quad 0 \leq z \leq z_{max}, \quad z_{j+1} = z_j + \eta_{j+1}, \quad j = 0 \dots M_i - 1\}. \end{aligned} \quad (10)$$

The spatial finite difference operator is:

$$\Lambda_i [\widehat{T}_{i,j}] = \frac{1}{r_i} \frac{1}{\widehat{h}_i} \left[r_{i+\frac{1}{2}} \lambda_{i+\frac{1}{2},j} \frac{\widehat{T}_{i+1,j} - \widehat{T}_{i,j}}{h_{i+1}} - r_{i-\frac{1}{2}} \lambda_{i-\frac{1}{2},j} \frac{\widehat{T}_{i,j} - \widehat{T}_{i-1,j}}{h_i} \right], \quad (11)$$

$$\Lambda_j [T_{i,j}] = \frac{1}{\eta_j} \left[\lambda_{i,j+\frac{1}{2}} \frac{T_{i,j+1} - T_{i,j}}{\eta_{j+1}} - \lambda_{i,j-\frac{1}{2}} \frac{T_{i,j} - T_{i,j-1}}{\eta_j} \right], \quad (12)$$

where $i = 1 \dots N_j - 1$, $j = 1 \dots M_i - 1$, $h_i = r_i - r_{i-1}$, $\eta_j = z_j - z_{j-1}$, $\widehat{h}_i = 0.5(h_{i+1} + h_i)$, $\eta_j = 0.5(\eta_{j+1} + \eta_j)$, $T_{i,j} = T(r_i, z_j, t_k)$, $\widehat{T}_{i,j} = T(r_i, z_j, t_{k+1})$, $\lambda_{i,j} = \lambda_m(T_{i,j})$, $c_{V,i,j} = c_{V,m}(T_{i,j})$, $X_{i,j} = X_m(T_{i,j})$, $r_{i\pm\frac{1}{2}} = \frac{r_i + r_{i\pm 1}}{2}$, $\lambda_{i\pm\frac{1}{2},j} = \lambda_m\left(\frac{T_{i,j} + T_{i\pm 1,j}}{2}\right)$, $\lambda_{i,j\pm\frac{1}{2}} = \lambda_m\left(\frac{T_{i,j} + T_{i,j\pm 1}}{2}\right)$.

The indices i and j are global for the whole computational domain. The index m , which is marking the material, is chosen corresponding to the domain region, where from the pair (i, j) is taken.

The coefficients for the forward sweep of the Thomas algorithm [9, 10] are defined as:

$$\begin{cases} \alpha_i = \frac{-C_i}{B_i + A_i \alpha_{i-1}}, \\ \beta_i = \frac{F_i - A_i \beta_{i-1}}{B_i + A_i \alpha_{i-1}}, \end{cases} \quad (13)$$

The coefficients A_i , B_i , C_i and F_i are formulated from the difference equation Eq. (9):

$$\begin{cases} A_i = \frac{-r_{i-\frac{1}{2}} \lambda_{i-\frac{1}{2},j}}{r_i \widehat{h}_i h_i}, \\ B_i = \frac{1}{r_i \widehat{h}_i} \left[\frac{r_{i-\frac{1}{2}} \lambda_{i-\frac{1}{2},j}}{h_i} + \frac{r_{i+\frac{1}{2}} \lambda_{i+\frac{1}{2},j}}{h_{i+1}} \right] + \frac{\rho_{i,j} c_{V,i,j}}{\tau}, \\ C_i = \frac{-r_{i+\frac{1}{2}} \lambda_{i+\frac{1}{2},j}}{r_i \widehat{h}_i h_{i+1}}, \\ F_i = \frac{\rho c_{V,i,j}}{\tau} T_{i,j} + \Lambda_j [T_{i,j}] + X_{i,j}. \end{cases} \quad (14)$$

Finally, the following formula has been used to calculate unknown values of $\widehat{T}_{i,j}$:

$$\widehat{T}_{i,j} = \alpha_i \widehat{T}_{i+1,j} + \beta_i. \quad (15)$$

For the forward sweep Eq. (13–14) and back sweep Eq. (15), one needs to initialize values α_0 , β_0 and $\widehat{T}_{N_j,j}$ respectively. These values have to be initialized to satisfy the boundary conditions.

Note that in the case of a non-uniform grid or discontinuities of the first kind of the thermal coefficients, scheme (9) has the first order difference approximation via spatial coordinates¹ [5, 8].

¹Actually, the order of difference approximation depended on choice of a norm [5, 8].

Therefore, for approximations of the boundary and conjugation conditions, it is enough to use the difference approximation of the first order.

The boundary conditions have been approximated by the following set of formulas:

$$\begin{cases} \widehat{T}_{0,j} = \widehat{T}_{1,j} \\ \widehat{T}_{N_j,j} = \widehat{T}_{N_j-1,j}, \end{cases} \quad (16)$$

for $r = 0$ and $r = r_{\max}$, respectively. Difference approximations of the other boundary conditions can be constructed in a similar way.

The initial values of α and β are defined in such a way as to satisfy the boundary conditions (16):

$$\alpha_0 = 1, \quad \beta_0 = 0. \quad (17)$$

To initialize the recursive formula (15), taking into account the boundary conditions Eq. (16), the $T_{N_r,j}$ is calculated as:

$$\widehat{T}_{N_j,j} = \frac{\beta_{N_j-1}}{1 - \alpha_{N_j-1}}. \quad (18)$$

The relations on the border between layers are given in the form

$$\begin{cases} \widehat{T}_{i^*-0,j} = \widehat{T}_{i^*+0,j}, \\ -\lambda_m(T_{i^*-0,j}) \frac{T_{i^*,j} - T_{i^*-1,j}}{h_{i^*}} = -\lambda_{m+1}(T_{i^*+0,j}) \frac{T_{i^*+1,j} - T_{i^*+0,j}}{h_{i^*+1}}, \end{cases} \quad (19)$$

Here we use the following notation: $\widehat{T}_{i^*,j} = \widehat{T}_{i^*+0,j} = \widehat{T}_{i^*-0,j}$ and $\lambda_m^* = \lambda_m(T_{i^*,j})$. Instead of the recursive formula Eq. (15), after a simple transformation, a similar function can be expressed at the discontinuity point as:

$$\widehat{T}_{i^*,j} = \alpha_{i^*} \widehat{T}_{i^*+1,j} + \beta_{i^*}. \quad (20)$$

From Eq. (19), the coefficients for the forward sweep of the Thomas algorithm, α_{i^*} and β_{i^*} , can be represented as follows:

$$\begin{cases} \alpha_{i^*} = \frac{\lambda_{m+1}^* h_{i^*}}{\lambda_{m+1}^* h_{i^*} + \lambda_m^* h_{i^*+1} (1 - \alpha_{i^*-1})}, \\ \beta_{i^*} = \frac{\lambda_m^* h_{i^*+1} \beta_{i^*-1}}{\lambda_{m+1}^* h_{i^*} + \lambda_m^* h_{i^*+1} (1 - \alpha_{i^*-1})}. \end{cases} \quad (21)$$

The difference scheme (9-21) has unconditional stability related to spatial step h_i and conditional stability related to η_j [11]:

$$\tau \leq \frac{\min |\eta_j|}{2} \min \left| \frac{\rho(T, r, z) c_V(T, r, z)}{\lambda(T, r, z)} \right|. \quad (22)$$

Generally, the conditional stability could be a strong limitation for the practical usage of a difference scheme. However, our scheme is practical in the cases where spatial step is sufficiently

large in one direction, moreover where the step in other direction is too small, which takes place in our model.

Of course, one could discuss the Alternating Direction Implicit (ADI) method [5, 10, 12] which is absolutely stable with relation to the choice of spatial step. The motivation for our choice of method derives from the relative simplicity of technical realization when compared to ADI and the natural affinity for parallel computing (parallelization in direction when it has conditional stability).

3.1. Model of Transient Process for Source Term

Generally, for implicit difference schema with coefficients depending on the sought-after function (temperature), one needs to make iterations for evaluation of temperature at each time step (for example, using Newton method) [5].

Without using iterations, implementation of the schema Eq. (9-21) at the moment of noncontinuous switch on of source (like a theta function) can lead to a jump of the temperature depending on the amplitude of source (see Fig. 3b). Of course, the choice of sufficiently small time-step will avoid that problem without using iterations. However, we introduce another more physically motivated method to solve this problem, namely the transient process. However, we can avoid such behavior of temperature without using iterations by introducing transient process model of source switching on.

Formally, it can be done with a choice the function (Fig. 2)

$$p^2(t) = 1 - \exp\left(\frac{t - nt_{prd}}{7\tau^*}\right) \quad (23)$$

instead of $p^2(t) \equiv 1$. Here $\tau^* = \tau/100$, and the number 7 is introduced to have saturation occurring approximately in the middle of the time interval τ (7 is a magic number in relation to 100).

The transient process is realized in the following way. When the source is switched on (see Eq. (5)), it starts at each moment $t = nt_{prd}$. We performed the calculations with time-step τ^* up to $t = nt_{prd} + \tau$. Further, calculations continue with time-step τ and $p^2(t) \equiv 1$ up to $t = (n + 1)t_{prd}$. Then the transient process repeats.

In Fig. 5, comparison between two calculations made with (left figure) and without (right figure) the transient model is shown. Even the behavior of the solutions are completely different. In the incorrect solution (without transient model 3b), the temperature has a big jump and then the system starts to cool down instead of monotonic heating, which is the correct solution (with the transient model 3a). The implementation of the transient model method shows that this model is very economical.

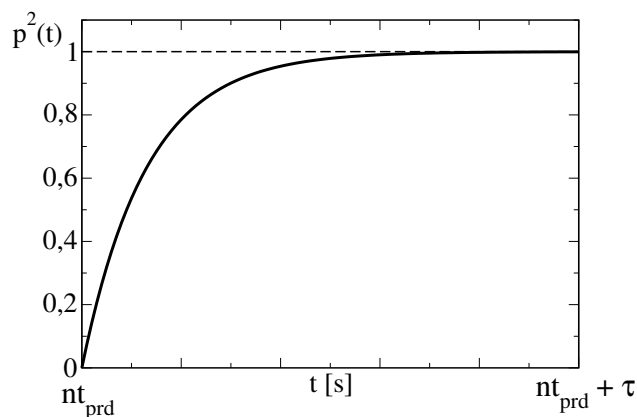


Figure 2: Transient model function.

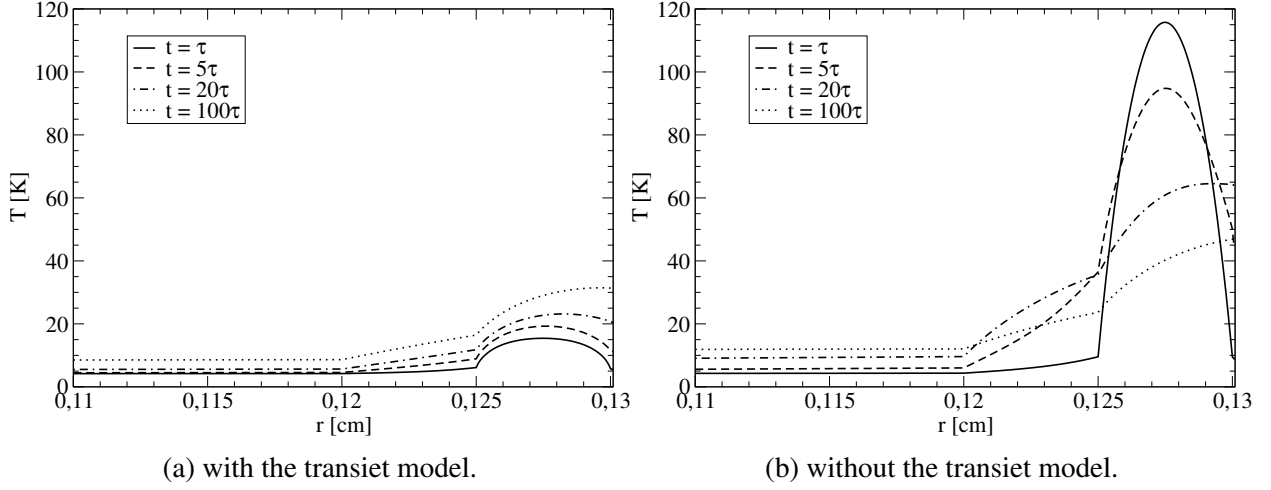


Figure 3: Comparison calculations with transient model and without it.

4. OpenCL Realization of the Algorithm

The OpenCL realization of the numerical algorithm, described in the previous section, is based on the following idea. In each time step, the cycle for j -index from 1 to $M - 1$ is parallelized. Each called thread simultaneously calculates the sought-after function by the Thomas algorithm, see Fig. 4. In the figure, we show the discretization of the function domain. Particularly, we group a set of points corresponding to one j^{th} thread. We also show the points involved in the calculation of the given (i, j) point (bold point and crossed points on the Fig. 4).

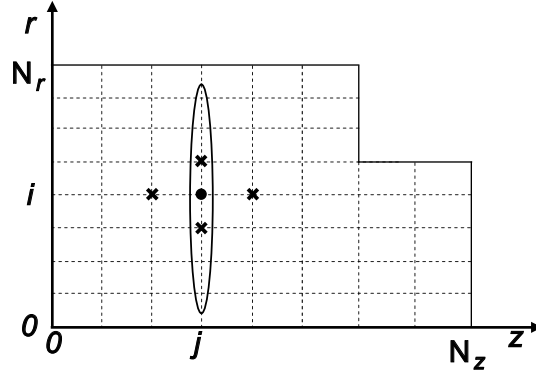
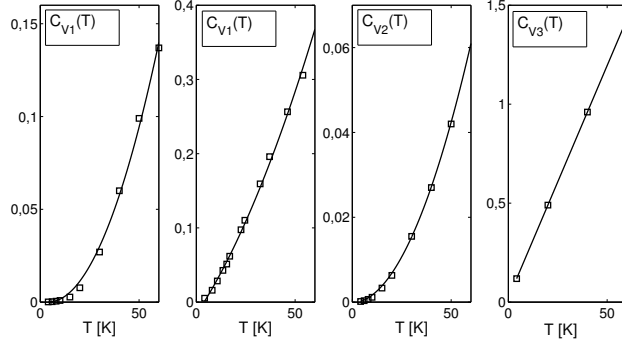


Figure 4: Schematic representation of discretization of the function domain.

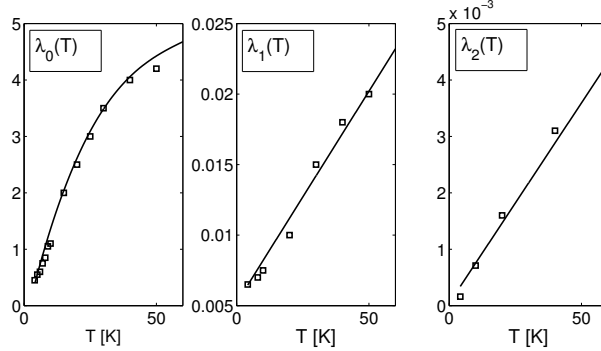
5. Results and Discussion

In this work we discuss the results of the numerical simulations only for one particular choice of the configuration of the object (Fig. 1). Its geometrical characteristics have been taken as follows: $r_0 = 0.12$ cm, $r_1 = 0.125$ cm, $r_2 = 0.13$ cm, $r_{\text{max}} = 0.1301$ cm, $z_0 = 4$ cm, $z_{\text{max}} = 5$ cm.

The temperature dependencies of thermal coefficients, c_{V_m} specific heat capacity and λ_m thermal conductivity, for each materials are given as it is shown in Fig. 5a and Fig. 5b. For the chosen materials the corresponding data points have been taken from [13]. These dependencies have been fitted by the least-squares method using polynomial functions. For the external insulator (fourth material: $m = 4$), we took the thermal conductivity to be constant $\lambda_4 = 10^{-3} \text{ J}/(\text{gK})$. The densities of the chosen materials are $\rho_0 = 8.92$, $\rho_1 = \rho_2 = 2$ and $\rho_3 = 2.5$ in units g/cm^3 . It is easy to see that thermal coefficients vary up to a few orders of magnitude as temperature varies in cryogenic diapason. It makes the choice of the time-step more sensitive on the values of temperature (sought-after function) (see condition (22)), for this concrete configuration, the suitable time-step is $\tau = 10^{-5}$ sec. The period of source switching is $t_{\text{prd}} = 25$ ms, where the heating time is $t_{\text{src}} = 1$ ms Eq. (4), and electric current amplitude is $I_0 = 10^2$ mA Eq. (5). The critical value of temperature is taken as $T_{\text{crit}} = 42$ K (temperature of evaporation of working gases). The initial temperature has been taken to be equal $T_0 = 4.2$ K.



(a) The heat capacities for different materials, $c_V(T)$ [$\text{J}/(\text{g} \cdot \text{K})$].



(b) The thermal conductivities for different materials, $\lambda(T)$ [$\text{W}/(\text{cm} \cdot \text{K})$].

Figure 5: Temperature dependencies of thermal coefficients.

Note that because of the structural features of the object, especially because of existence of tiny layers covering the core cylinder, the choice of spatial step in the radial direction has to be less in comparison to the size of the layers (at least in order of magnitude) to guarantee the stable solution. Therefore our choice of the difference scheme (see Section 3), which is suitable for the technical realization, is justified.

5.1. Results of Numerical Simulations

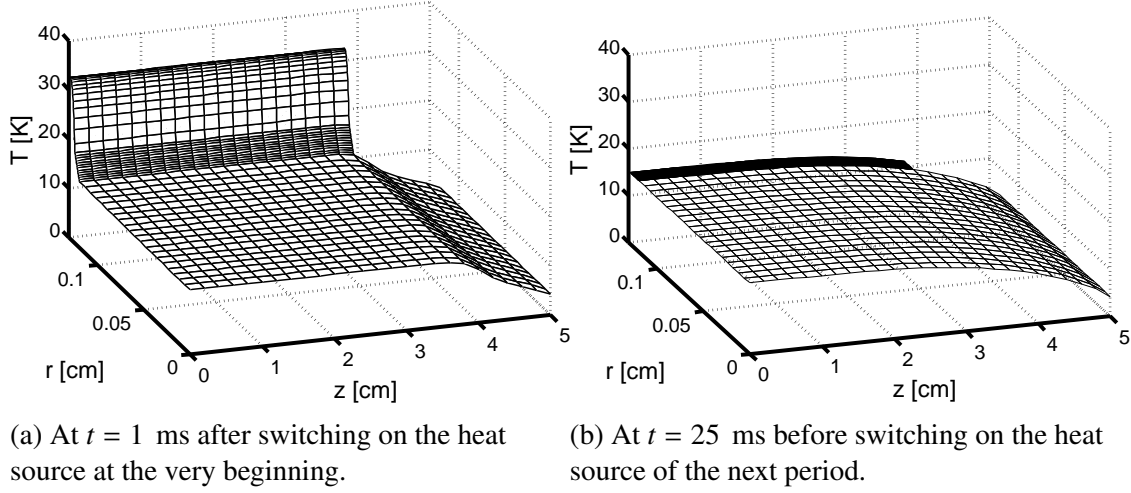


Figure 6: Temperature profile $T(r, z)$ at different times.

In Fig. 6, we show the temperature profiles at the very beginning. The temperature inside the object at $t = 1$ ms is shown in the left panel (see Fig. 6a). At the same moment, the source is switching off in the first period of source function. Because the radius of the cylinder is much smaller than its length, the heat first flows to the central axis and then to the right border, where the cryostat (the liquid helium temperature terminal) is located at $z_{\max} = 5$ cm.

At the right panel of Fig. 6b, we show the temperature distribution at $t = 25$ ms (after first period). One period of the source switching T_{prd} is enough time to equilibrate the temperature in radial direction (see Fig. 6b). On the other hand, the period of time is not enough to relax the temperature to the value right before switching on the source (see Figs. 7a,7b,7c). Such behavior repeats for approximately 10 sec (setting time) until a stable periodic regime is achieved (see Fig. 7d). The setting time varies depending on design of the object and switching time of the source.

For applications, it is very important that the maximum value of the temperature T_{\max} achieves higher value than the critical value of evaporation of working gases ($T_{\text{crit}} \approx 42$ K) and distributed along almost the whole working surface ($r = r_{\max}$, $z \in [0 \dots z_0]$) (Fig. 8). The maximum value of the minimal temperature in the stable regime is less than the critical one (Fig. 8), as it is required.

Moreover, the width of the temperature peaks is approximately 1 – 1.5 ms and is much smaller in comparison with the whole period (Fig. 7b), which allows for working gases to condensate on the surface before the next evaporation.

In the Fig. 8 easy to see, that in our particular case, the 75% (approximately) of working surface is actually useful. This percentage can be controlled, for example, with a proper choice of the amplitude of electric current I_0 . In principle, this equation mathematically can be formulated as source control problem, which can help to raise the efficiency.

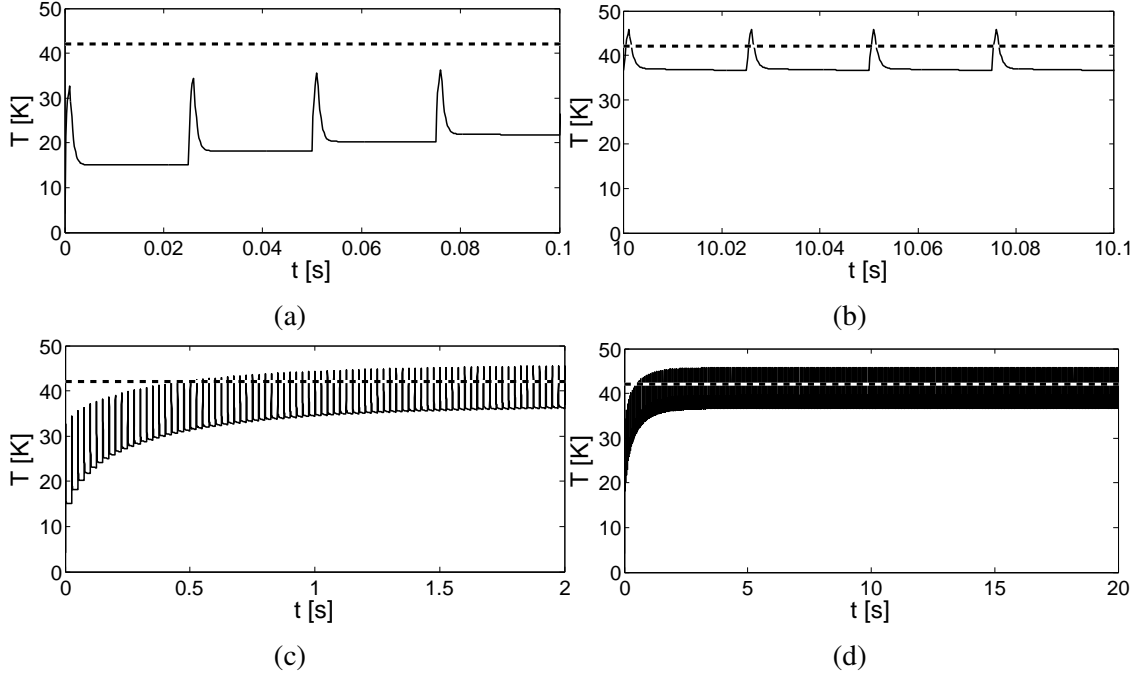


Figure 7: Time evolution of the surface temperature at $z = 0$ (solid line), critical temperature for evaporator and condensation of working gas (dashed line).

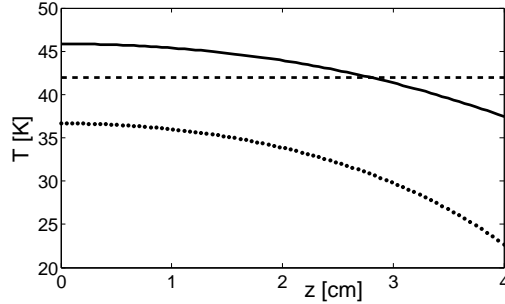


Figure 8: Temperature profiles at the stable regime just before at moments of source switching on (dot line) and switching off (solid line). The critical temperature (dashed line).

5.2. Results of the OpenCL algorithm

The time calculations for different $N \times M$ are given in the Table 1 (here and in the table: $N = \max_j N_j$ and $M = \max_i M_i$). To demonstrate the results of OpenCL algorithm the calculations have been done for temperature evolution from $t = 0$ sec. up to $t = 0.0765$ sec. with time step $\tau = 10^{-6}$ sec. In the table we use following notations: **CPU** – Core i7 3517U (Ubuntu 11.0) and **GPU** – GF GTX 470 (Core 2 Duo, Debian 6.0). During the compilation of programs -O2 optimization flag have been used. It is shown that there is an interval of increasing number of points of discretization in axial direction (M) where the calculation time using GPU remains the same. In the Table 1, we compare of calculation times for *CPU* and *GPU* using 3 different grids

with the same $N = 431$ and two with same $M = 401$. So, the choice of our algorithm allows for us to increase the density of our computational grid in the axial direction, practically without loss of calculation time.

Table 1: Calculation time of OpenCL algorithm for different grid size.

$N \times M$	CPU	GPU
431×101	309 sec.	345 sec.
431×201	607 sec.	349 sec.
431×401	1315 sec.	357 sec.
631×401	1968 sec.	509 sec.

6. Conclusion

We have suggested a model of temperature evolution for a multilayer cylindrical object, which is a device for pulse feeding (in the millisecond range) the working gases into the working space of the ion source.

The algorithm for simulation of heat conduction process with a periodical source in cylindrical multilayer object and its OpenCL realization have been developed. It is based on explicit–implicit method. Because of the structural features of the device, the choice of the difference scheme is suitable for the technical realization.

For the stability of simulations, the transient process model for source switching is introduced.

It is shown that the temperature regime in the object can be conditionally divided in two parts. The first part is a setting mode (around 10 sec.). Here the needed temperature regime at the surface of the object has not yet been established. The second part is a working mode. Here the needed temperature regime at the surface has been already established.

The mean value of the temperature over the surface changes around the critical one periodically in the interval of $32 \text{ K} \lesssim T \lesssim 43.5 \text{ K}$ ($T_{\text{crit}} = 42 \text{ K}$). The key characteristics of the device working thermal process is achieved by a particular choice of the model parameters.

Acknowledgements

Authors thank Dr. Edik Ayryan (JINR), Dr. Ján Buša, Dr. Imrich Pokorný (TU of Košice, Slovakia), Mark A. Kaltenborn and Prof. David Blaschke (University of Wrocław) for useful advice and technical help. The calculations were done on the cluster Hybrilit – the heterogeneous computational system of Laboratory of Information Technology (<http://hybrilit.jinr.ru/>). The research was supported by JINR grant No. 14-602-01 and RFBR grants 11-01-00278 and 14-01-31227.

References

- [1] D.E. Donets et al, Electron-string ion sources of highly charged ions with linear and tubular geometry of string, Appl. Phys. 3 (2010) 34–41 (in russian)

- [2] D.E. Donets, E.E. Donets, T. Honma, K. Noda, A.Yu. Ramzdorf, V.V. Salnikov, V.B. Shutov, E.D. Donets. Physics research and technology developments of electron string ion sources, *Rev. Sci. Instrum.* 83 (2) (2012) 02A512
- [3] A. Ayriyan, J. Pribiš, Mathematical Simulation of Heat Conductivity in Composite Object with Cylindrical Symmetry, *Matem. model.* 24 (12) (2012) 113–118 (in Russian)
- [4] A. Ayriyan, E. Ayryan, E. Donets and J. Pribiš, Numerical Simulation of Heat Conductivity in Composite Object with Cylindrical Symmetry, *Lect. Notes Comput. Sci.* 7125 (2012) 264–269
- [5] A.A. Samarskii, P.N. Vabishchevich, *Computational heat transfer, Volume 1*, John Wiley & Sons Ltd., Chichester, England (1995)
- [6] P. Symons, *Digital Waveform Generation*, Cambridge University Press, New York (2013)
- [7] Z. Gajic, *Linear Dynamic Systems and Signals*, Prentice Hall, Upper Saddle River (2002)
- [8] A.A. Samarsky, *The Theory of Difference Schemes*, Marcel Dekker Inc., New York (2001)
- [9] L.H. Thomas, *Elliptic Problems in Linear Differential Equations over a Network*, Watson Sci. Comput. Lab Report, Columbia University, New York (1949)
- [10] W.H. Press, S.A. Teukolsky, W.T. Vetterling, B.P. Flannery, *Numerical Recipes*, third ed., Cambridge University Press, New York (2007)
- [11] N.N. Yanenko, *Fractional step methods for solution of multidimensional problems of mathematical physics*, Nauka, Moscow (1967) (in russian)
- [12] D.W. Peaceman, H.H. Rachford Jr., The numerical solution of parabolic and elliptic differential equations, *J. Soc. Ind. Appl. Math.* 3 (1) (1955) 28–41
- [13] National Institute Of Standards And Technology, <http://www.nist.com>